# Design of an HF-VHF Ice Penetrating Synthetic Aperture Radar

Jonathan D. Hawkins[#1], Paul V. Brennan[#], Keith W. Nicholls[†], Lai Bun Lok[#]

[#]Department of Electronic and Electrical Engineering, University College London, UK
[†]British Antarctic Survey, Cambridge, UK
[1]jonathan.hawkins.17@ucl.ac.uk

*Abstract* — **The design of an HF-VHF frequency modulated continuous wave radar intended for use with an autonomous rover in the polar regions is presented. The RF front-end, antenna design and deramped filter for the radar are described and validated using laboratory measurements and an outdoor field measurement.**

*Keywords* — **ice-penetrating radar, FMCW radar, dipole antenna**

## I. INTRODUCTION

Processes at the ice-ocean interface of polar ice shelves are of key importance to glaciologists, oceanographers and climate scientists studying the contribution of ice sheets to future sea level rise [1]. The stability of ice shelves can be undermined by subsurface topography such as melt channels and basal crevasses [2], [3] however changes in these features are difficult to observe directly, especially at the timescales of the oceanographic forcing.

Synthetic aperture radar (SAR) is an imaging technique that improves cross-range resolution, introduces a coherent gain and retains phase information which can be used in interferometric processing. Airborne SAR platforms are well established in the imaging of polar ice shelves [4], [5] however are generally not suited for monitoring temporal changes and limited in operation by good flying conditions during austral summer. Ground-based radars for ice imaging are typically high-power, phase-incoherent impulse radars [6], [7], [8], [9] that are unsuitable for use in SAR systems. With recent developments in polar rovers [10] [11] however, the concept of an autonomous ground-based SAR platform with sufficient phase (range) precision to monitor spatio-temporal changes in the basal interface of ice shelves can be investigated. A candidate radar that has such precision is the Autonomous phase-sensitive Radio Echo Sounder (ApRES) [12] which currently operates between 200 MHz and 400 MHz.

This paper describes a new ApRES radar design, including antennas, that operates from 20 MHz to 40 MHz. This increases the required spatial sampling interval to 1 m [13] which allows SAR surveys to be conducted across wider areas, at the cost of reduced vertical resolution ($\Delta R$) of 4.19 m in ice and increased antenna size. Wire-mesh dipole antennas [14] with improved matching are realised to retain a lightweight platform that meets the payload limit of polar rovers. Laboratory-based testing of the HF-VHF radar printed circuit board (PCB) and an outdoor measurement of the antennas are presented. A comparison of the HF-VHF ApRES SAR with other radar platforms is then provided.
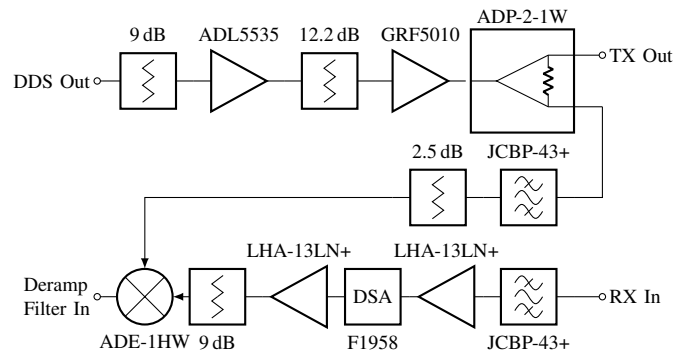


Fig. 1. Block diagram of the RF front-end for the HF-VHF ApRES.

## II. RADAR SYSTEM DESIGN

### A. RF Front End

The ApRES generates the linear frequency modulated continuous wave (FMCW) chirp using a direct digital synthesizer (DDS) which is user-programmable from near dc to 400 MHz. When the minimum chirp frequency is reduced to 20 MHz, the lower frequency limit of the amplifiers and the power de-rating of the digital step attenuator (DSA) for the RF front end must be considered.

Taking these factors into account, a new RF chain for the HF-VHF ApRES was devised as shown in Fig. 1. It has the same architecture as its VHF-UHF counterpart except the bandpass filters have been replaced with an HF-VHF equivalent (Mini-Circuits JCBP-43+) and the transmit amplifiers use a dual-stage gain configuration (Analog Devices ADL5535 and Guerilla RF GRF5010). Tuneable gain in the receive chain is realised using a digital step attenuator (Renesas F1958) between two low noise amplifiers (Mini-Circuits LHA-13LN+). The RF front-end has a link budget that is commensurate with the original VHF-UHF design. When combined with the radar microcontroller (Venom Control Systems VM2) the system has an idle current of 15 mA using a 12 V supply rising to 86 mA with Ethernet control enabled, and 460 mA during transmission which is suitable for long endurance usage with a polar rover to realise a large synthetic aperture size.

### B. Wire-Mesh Antenna

The antennas for the HF-VHF ApRES use the broadband wire-mesh dipole design [14] with a new matching network. This has been redesigned to improve the bandwidth and allow
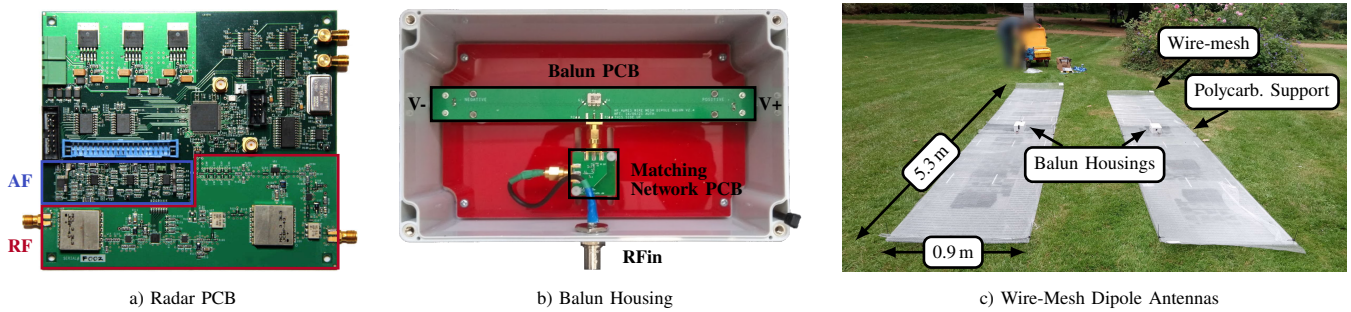
Fig. 2. Realised components of the HF-VHF ApRES. a) Radar PCB with modified deramped (AF) filter and RF front-end, b) Balun housing containing matching network PCB and balun PCB, c) Wire-mesh dipole antennas assembled on polycarbonate supports.

for the option of mounting the antennas on sledges to facilitate rover-driven SAR deployment in a polar environment.

Nansen sledges are commonly available in polar research stations and have been used as the intended mount for the antenna. A simulation model of the wire-mesh dipole, a typical 3 m sledge and 10 mm thick twin-wall polycarbonate support structure was created in SIMULIA CST Studio 2020 to determine the expected impedance and radiation pattern, which are comparable to previously reported values [14].

*1) Matching Network*

The mean magnitude of the simulated antenna impedance over the radar signal bandwidth (20 – 40 MHz) is 160 Ω. A transformer (Mini-Circuits ADT4-6T+) with a 1:2 turns ratio was chosen to minimise the return loss of the wire-mesh dipole over the same bandwidth, when referred to a 50 Ω source.

Measured *s*-parameters of the Mini-Circuits transformer were cascaded with the simulated *s*-parameters from the electromagnetic model of the Nansen sledge-mounted antenna and used as the input to Keysight's Advanced Design System Impedance Matching tool to generate a 5th order passive *LC* matching network for the 50 Ω radar port impedance. This was found to be the minimum order to yield an $S_{11}$ of less than −10 dB over the radar signal bandwidth. The *LC* matching network is shown in Fig. 3 alongside the transformer and feed lines to the wire-mesh dipole antenna.

The feed lines are implemented as 50 Ω coplanar waveguide transmission lines on 1.6 mm FR-4 substrate. Separate PCBs for the balun and matching network were chosen to enable measurement of the unmatched wire-mesh dipole impedance in the field and to allow users the option of



Fig. 3. Schematic for balun housing comprising a) fifth-order *LC* matching network PCB and b) balun PCB with 100 mm transmission lines.

replacing the matching network, for example, when deploying the radar in alpine or waterlogged glacier conditions.

*C. Deramped Signal Filter*

The frequency response of the deramp filter in an FMCW radar is designed to apply a range-dependent gain of $40 \, \text{dB decade}^{-1}$ to the deramped signal to compensate for path losses and maximise dynamic range at the analogue to digital converter. For a point target, the deramp frequency is given by

$$f_d = \frac{2BR\sqrt{\varepsilon_r}}{c_0 T}, \quad (1)$$

where $R$ is the one-way range to the target, $B$ is the chirp bandwidth, $T$ is the chirp duration, $c_0$ is the speed of light in a vacuum and $\varepsilon_r$ is the relative permittivity of the (lossless) propagation medium. The ten-fold reduction in bandwidth for the HF-VHF ApRES means that the original range-frequency characteristic [12] is shifted downwards by a decade (if all other parameters are kept the same). Although this can be compensated by reducing the chirp duration $T$ accordingly, it would trade-off with a reduced SNR (for the same number of coherently summed chirps).

To optimize the range-frequency characteristic in hardware for HF-VHF radar operation while maintaining a chirp duration of 1 s, the deramp filter component values were modified to shift its peak gain response from 2.83 kHz to 419 Hz.

III. EXPERIMENTAL RESULTS

The realised components for the HF-VHF ApRES are shown in Fig. 2. The radar PCB was fabricated on a 4-layer FR4 substrate. For a DDS current setting of 20.07 mA the radar transmit output power is nominally 19.0 ± 1.1 dBm over the chirp bandwidth. The CW power spectra in Fig. 4a were measured using a Rohde & Schwarz FSU spectrum analyzer. The wideband spurious free dynamic range (SFDR) of an FMCW ramp is derived from Fig. 4b as 20.5 dB from dc to 100 MHz, measured using a Keysight N9915A FieldFox in spectrum analyzer mode. Resolution and video bandwidths were increased in Fig. 4b to ensure the peak output power was sampled sufficiently throughout the FMCW ramp. Decreasing the DDS current to 8.64 mA reduces the radar transmit output power to 12.4±1.8 dBm and increases the SFDR of the FMCW
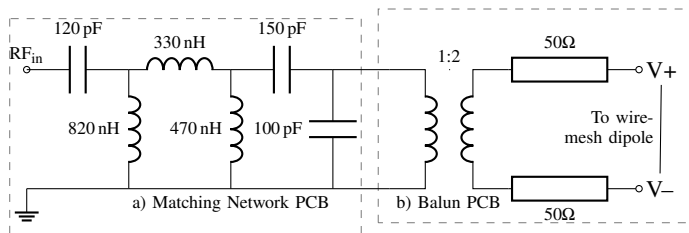
ramp to 27.5 dB. The DDS current is user-programmable in steps of 90 μA from 8.64 mA to 20.07 mA. The relationship between DDS current, transmitted power and dynamic range is non-linear and not recommended for use as a user-configurable parameter of the radar.

Fig. 5a shows a measured range profile, expressed as deramped frequency using (1), with a 240 m length of coaxial cable (Huber & Suhner, S_04272_B, $\varepsilon_r = 1.49$) connected in series with 78 dB of fixed attenuation between the radar TX and RX ports. The -40 dBV amplitude tone at 20 Hz corresponds to the overall path gain and half the length of the loop cable respectively.

With the radar configured in this loopback mode, the magnitude response of the deramped filter was measured by varying $T$ in discrete steps. Fig. 5b shows a good agreement with the response simulated in SPICE. Measurements at deramped frequencies below 7.5 Hz require long chirp periods where the number of 16-bit ADC samples at 40 kHz exceed the available RAM (<1 MB) in the radar microcontroller.

Fig. 2c shows the assembled wire-mesh dipole antennas without the Nansen sledges. The antenna structure is de-mountable and the dipole elements can be rolled up [15] such that a pair of HF-VHF antennas is transportable within a volume of 1 m × 0.9 m × 0.3 m and weighing 32 kg. The reflection coefficient of the constructed antenna was measured when positioned at ground level on silty loamy soil, as an analogue to the intended glacier environment. Fig. 6 compares the calibrated $S_{11}$ measured for the antenna with simulation results assuming a dielectric half-space of relative permittivity of 2.44 and loss tangent 1.7. The measured reflection coefficient of the wire-mesh dipole antenna satisfies the 20-40 MHz bandwidth for $|S_{11}|$ less than −10 dB which is improved upon an earlier design [14].

Table 1 compares fundamental system parameters of the HF-VHF ApRES with contemporary ground-based or autonomous imaging radar platforms using a metric of normalised power $P_N$, calculated as the product of transmit power, transmit duration and pulse-repetition frequency. The
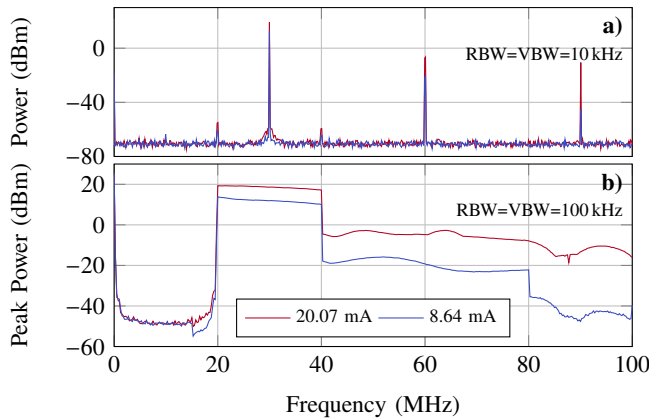


Fig. 4. Comparison of output spectra for maximum and minimum DDS current during a.) CW tone at 30 MHz with and b.) 1 s 20-40 MHz FMCW ramp in peak hold mode..
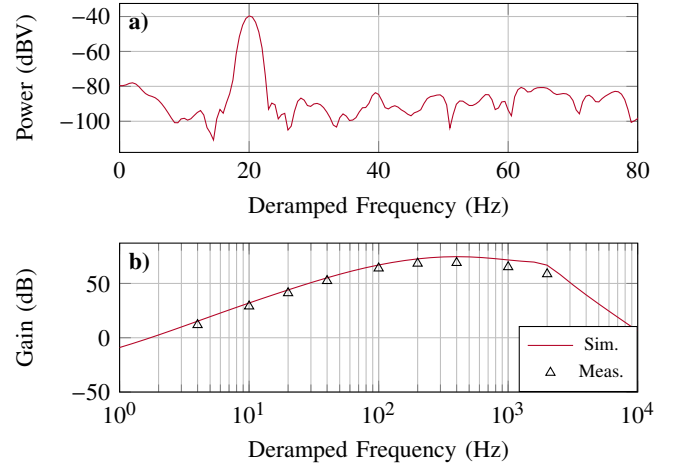


Fig. 5. a) Range profile from loopback test ($T = 1$ s, averaged over 10 chirps), b) Magnitude response for the deramped filter.
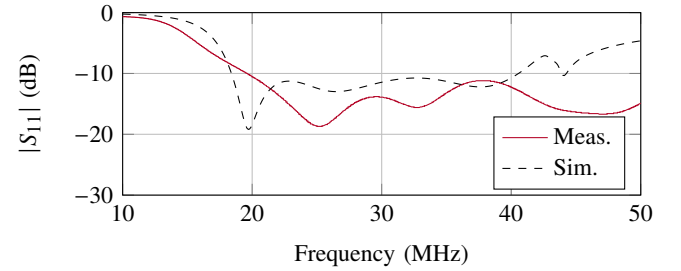


Fig. 6. Input reflection coefficient for the wire-mesh dipole antenna positioned on soil at ground-level.

maximum sounding range ($R_m$) for this work is subject to field validation, but is expected to compete with that reported in [8] for a lower transmit power $P_{TX}$ and smaller size.

## IV. Conclusion

The design and testing of a new HF-VHF ApRES radar PCB and its accompanying antenna have been described, demonstrating its suitability for use in a low-power, autonomous rover-towed radar system. Antarctic field-trials took place in January 2022 from which results are currently in preparation.

Table 1. Comparison with state-of-the-art ice-penetrating radars.

| Ref. | Platform | Centre Freq. (MHz) | $R_m$ (m) | $\Delta R$ (m) | $P_{TX}$ (W) | $P_N$ (W) |
|---|---|---|---|---|---|---|
| [5] | Drone | 14.6 | 500 | 84.06 | 100 | 1.0 |
|  | Drone | 34.3 | 500 | 16.81 | 100 | 0.32 |
| [8] | Pistenbully | 750 | 2,800 | 0.28 | 800 | 80 |
| [11] | Rover | 400 | 344 | 0.21 | 260 | 0.33 |
| This Work | Rover | 30 | - | 4.19 | 0.1 | 0.1 |

## References

[1] G. H. Gudmundsson, "Ice-shelf buttressing and the stability of marine ice sheets," *The Cryosphere*, vol. 7, no. 2, pp. 647–655, 2013.

[2] A. M. Le Brocq *et al.*, "Evidence from ice shelves for channelized meltwater flow beneath the Antarctic Ice Sheet," *Nature Geoscience*, vol. 6, no. 11, pp. 945–948, 2013.

[3] P. Dutrieux *et al.*, "Basal terraces on melting ice shelves," *Geophysical Research Letters*, vol. 41, no. 15, pp. 5506–5513, Aug 2014.

[4] A. Winter *et al.*, "Comparison of measurements from different radio-echo sounding systems and synchronization with the ice core at Dome C, Antarctica," *Cryosphere*, vol. 11, no. 1, pp. 653–668, 2017.

[5] E. Arnold *et al.*, "CReSIS airborne radars and platforms for ice and snow sounding," *Annals of Glaciology*, pp. 1–10, 2019.

[6] E. C. King *et al.*, "DELORES Mark 1: Construction and operation of the British Antarctic Survey Deep Look Radio Echo Sounder," in *International Conference on Radioglaciology and its applications*, Madrid, 2008.

[7] L. Mingo *et al.*, "A stationary impulse-radar system for autonomous deployment in cold and temperate environments," *Annals of Glaciology*, pp. 1–9, 2020.

[8] J. A. Nunn *et al.*, "A Lightweight Planar Ultrawideband UHF Monopole Mills Cross Array for Ice Sounding," *IEEE Antennas and Wireless Propagation Letters*, vol. 19, no. 7, pp. 1197–1200, 2020.

[9] T. R. Hillebrand *et al.*, "Radio-echo sounding and waveform modeling reveal abundant marine ice in former rifts and basal crevasses within Crary Ice Rise, Antarctica," *Journal of Glaciology*, pp. 1–12, 2021.

[10] A. O. Hoffman *et al.*, "A low-cost autonomous rover for polar science," *Geoscientific Instrumentation, Methods and Data Systems*, vol. 8, no. 1, pp. 149–159, 2019.

[11] K. D. Mankoff *et al.*, "Search and recovery of aircraft parts in ice-sheet crevasse fields using airborne and in situ geophysical sensors," *Journal of Glaciology*, vol. 66, no. 257, pp. 496–508, 2020.

[12] P. V. Brennan *et al.*, "Phase-sensitive FMCW radar system for high-precision Antarctic ice shelf profile monitoring," *IET Radar, Sonar & Navigation*, vol. 8, no. 7, pp. 776–786, 2014.

[13] N. Holschuh, K. Christianson, and S. Anandakrishnan, "Power loss in dipping internal reflectors, imaged using ice-penetrating radar," *Annals of Glaciology*, vol. 55, no. 67, pp. 49–56, 2014.

[14] J. D. Hawkins *et al.*, "HF Wire-Mesh Dipole Antennas for Broadband Ice-Penetrating Radar," *IEEE Antennas and Wireless Propagation Letters*, vol. 19, no. 12, pp. 2172–2176, 2020.

[15] A. Traille *et al.*, "A conformal/rollable monolithic miniaturized ultra-portable ground penetrating radar using additive and inkjet printing," in *IEEE MTT-S International Microwave Symposium*, Tampa, FL, USA, Jun 2014, pp. 1–4.